Materials Research. 2020; 23(2): e20200067
DOI: https://doi.org/10.1590/1980-5373-MR-2020-0067

Effect of Laser Power and Substrate on the Hastelloy C276™ Coatings Features Deposited by Laser Cladding

Lubar Eduardo Hortmann Santos Rivero[a] Alex Pizzatto[a], Moises Felipe Teixeira[b], Alexsandro Rabelo[b], Tiago Falcade[c], Adriano Scheid[a*]

[a]*Universidade Federal do Paraná, Programa de Pos-Graduação em Engenharia Mecânica - PGMEC, Av. Cel. Francisco H. dos Santos, 210, Curitiba, PR, Brasil*

[b]*Instituto SENAI de Inovação (ISI-SENAI), R. Arno Waldemar Dohler, 308, Joinville, SC, Brasil*

[c]*Universidade Federal do Rio Grande do Sul - UFRGS, Departamento de Físico-Química, Programa de Pós-Graduação em Engenharia de Minas, Metalúrgica e de Materiais – PPGE3M, Av. Bento Gonçalves, 9500, Porto Alegre, RS, Brasil*

Received: February 17, 2020; Revised: April 2, 2020; Accepted: April 14, 2020

Laser power influences the range of dilution with the substrate and thus, the microstructure and properties of the coatings. This work evaluated the effect of laser power on the dilution, microstructure, hardness and wear behavior of Hastelloy C276™ alloy coatings deposited on AISI 304L stainless steel and GGG40 ductile iron. The microstructure was comprised of γ (Ni-FCC) dendrites and molybdenum-rich interdendritic regions containing carbides. The coatings showed similar second phase nature and fraction and equivalent hardness and wear behavior for the lowest laser power condition. Otherwise, higher power on 304L induced to a lower fraction of blocky-like $M_{23}C_6$/MC carbides; whilst on GGG40 led to a higher fraction of a predominantly lamellar M_6C type carbide. Largely diluted coatings on ductile iron entailed differences in the strengthening mechanisms which led to higher hardness and lower wear rate. Moreover, wear tracks showed surface oxidation which in turn negatively influenced the performance of specimens with low dilution on both substrates. On the other way, with high dilution, this feature was only observed on stainless steel.

Keywords: *Laser Cladding, Hastelloy C276™, Dilution, Microstructure, Hardness, Wear Behavior, AISI 304L stainless steel, GGG40 ductile iron.*

1. Introduction

Different coating technologies have been adopted as a way to form protective layers at the surface of industrial components. Such layers commonly increase the service life of structural parts or tools exposed to aggressive environments. Beyond wear resistance under adhesion or abrasion, corrosion can take place sometimes farther, creating aggressive and complex degradation mechanisms. In this context, iron, as well as cobalt and nickel-base alloys, are often selected[1].

Among nickel alloys, Hastelloy C276™ stands out for its high amount of molybdenum, which leads to the highest resistance to pitting corrosion. Furthermost, it presents high strength even without heat treatment because of tungsten and molybdenum act as solid solution hardeners[2]. Taking into account these elements are also strong carbide formers, the second phase fraction may be altered due to the alloy dilution with the substrate during deposition. A sort of recent studies has pointed out interesting results concerning the dilution effect on coating properties. Some authors observed a significant increase in the mechanical properties of the coatings (e.g. hardness and wear resistance) when a carbide former-containing alloy is deposited on a high-carbon content substrate[3-5]. Otherwise, high dilution processing on low carbon substrates usually induces a drop in mechanical properties[3,6,7]. Therefore, the above-mentioned works highlight the importance of material selection for both clad and substrate, once it usually helps to predict coatings microstructure and properties.

Laser cladding has been drawing researcher's attention in recent years as a coating technology where a laser source simultaneously melts the substrate surface and the coating alloy precursor (powder or wire) to form a protective layer[8-11]. In most cases, the process has been set aiming for low dilution to produce minimum substrate melting then ensuring controlled chemical composition and metallurgical bonding. In this case, the deposited layer shows chemical composition and properties similar to those of the feeding alloy. Moreover, facing the low and localized heat input of this process, the coating solidifies under high cooling rates and therefore, resulting in largely refined microstructures[8,9].

Metallurgical features of laser cladding coatings are notably distinct from those processed, for instance, by

* e-mail: scheid@ufpr.br (Adriano Scheid)

conventional plasma spraying, due to the higher cooling rates during solidification[8,9]. This work aims to evaluate the microstructure and properties of Hastelloy C276™ single bead coating deposited by coaxial laser cladding on two different substrates. The effect of laser power, and therefore the dilution range, on the metallurgical and mechanical properties of the coatings, was also assessed.

2. Materials and Methods

Gas atomized Hastelloy C276™ (Hogänas) alloy powder with particle size ranging from 53 to 150 µm (Figure 1) was deposited by laser cladding with no substrate pre-heating using a coaxial nozzle on AISI 304L stainless steel and GGG40 (DIN 1693-73[12]) ferritic ductile iron plates 12,00 mm thick. The substrates were previously machined to get a flat surface free of irregularities from previous processing. Then, the surface was sandblasted to optimize laser energy absorption.

Table 1 presents the chemical composition of the materials studied in this work. Table 2 shows the main laser parameters adopted in a high-power Diode Laser (HPDL) PRECO™ SL8600 deposition center.

The coatings were deposited applying laser powers within 1.0- and 4.0-kW range with 0.5 kW increments as single-bead coatings with 80 mm length. They were first visually inspected and the adhesion with the substrate was evaluated. Deposits processed with 1.0 kW showed no adhesion i.e. no metallurgical bonding and they were discarded. From 1.5 kW on, good adhesion was achieved and further analyses were performed. Coatings characterization involved macro and micrographic analyses. Macrography was performed at the beginning, the center and the end of beads after taken 15 mm off from extremities. Wettability angle (θ), bead width (W) and reinforcement thickness (t) were determined by the methodology earlier purposed[3,8].

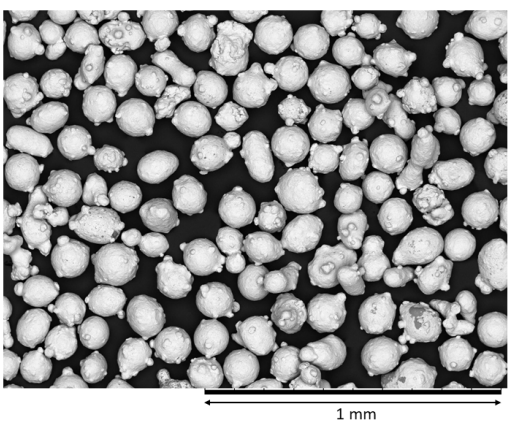

Figure 1. SEM image of the gas atomized Hastelloy C276™ particles.

The coatings dilution was assessed by macrographic areas analysis[3] and Toyserkani method[8], the later determines the dilution throughout iron measurements by energy dispersive spectrometry (EDS) at a scanning electron microscope (SEM) following the procedure adopted by Abioye et al.[13]. The EDS evaluation considered an area of 0,25 mm^2 selected inside the coating bead cross-section.

Microstructure description of polished samples was carried out in an SEM (TESCAN™ and ZEISS Supra™55VP) under backscattered electrons operational mode (BSE) on the top surface of the coatings. Phase fraction was determined with Image J™ software[14] applying a sequence of steps to get binary images (black and white) and then calculating the phase fraction. SEM images with 500X, 2000X and 5000X magnification – were adopted for phase quantification. X-ray diffraction analysis was performed to identify the phases formed in the coatings. There were adopted Kα-Cu radiation from 20 to 120° and the peak evaluation was supported by Crystallographica search-match (CSM™) software.

The Vickers hardness was evaluated under 1 kgf load in a Shimadzu HMV G21XY test machine. Wear behavior of the lowest and the highest dilutions for the coatings on both substrates was assessed via ball-on-flat reciprocating sliding wear tests in a CSM Instruments 1-124™ tribometer. A ZrO_2 sphere (6 mm diameter) slides under 5 N normal load on the top surface of the coatings which were flattened by machinery, grinding and polishing, as seen in Figure 2ab. A threshold of 120 m sliding distance was set up and the maximum travel speed was 20 mm/s. After the tests, the worn tracks were analyzed by scanning electron microscopy and white light interferometry (Alicona™ Infinite Focus G5 machine). Figure 3 shows the typical aspect of the tracks by these techniques. The worn volume was determined by way of subtracting the track 3D-profile from a reference plan (green area, Figure 3b).

Table 1. Materials chemical composition (wt.%)

Atomized Feeding Material									
Atomized Hastelloy C276™	**Ni**	**Cr**	**W**	**Mo**	**C**	**Fe**	**V**	**Si**	**Mn**
	Bal.	15.4	4.5	15.9	0.10	3.1	0.6	0.6	1.1
Substrate 1									
Hot Rolled AISI 304L	**Fe**	**C**	**Mn**	**Si**	**P**	**S**	**Cr**	**Ni**	**Mo**
	Bal.	0.02	1.3	0.4	0.04	0.001	18.1	8.0	0.1
Substrate 2									
Cast GGG40	**Fe**	**C**	**Mn**		**Si**	**P**		**S**	
	Bal.	3.9	0.1		2.8	0.02		0.03	

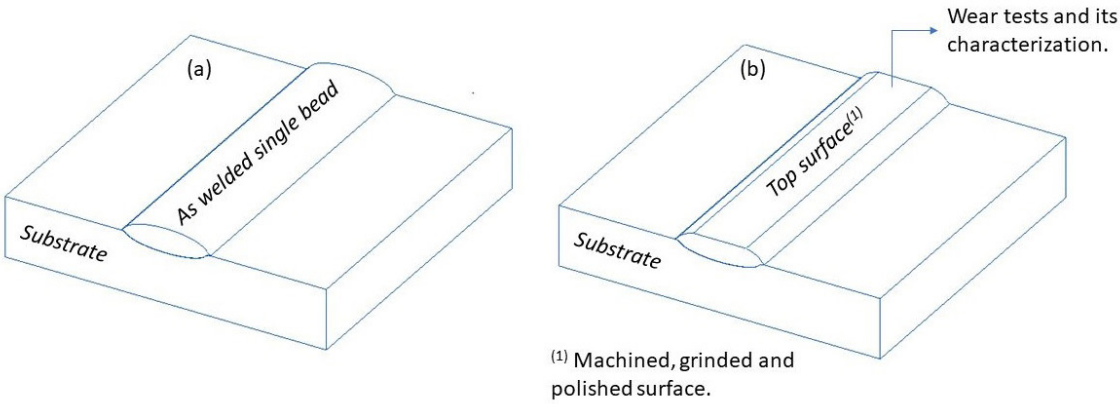

Figure 2. Schematic view of the as-deposited single bead (a) and the machined top surface (b).

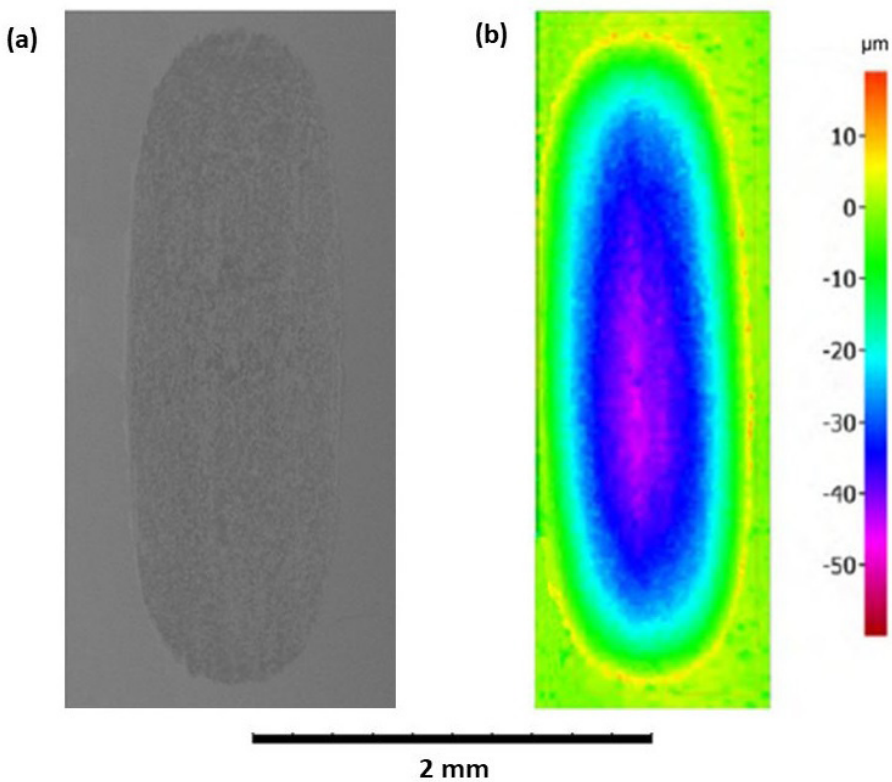

Figure 3. Typical SEM view of the worn track (a) and volume measurement using interferometry (b).

Table 2. Summary of laser parameters

Laser Type	High-power Diode Laser (HPDL)
Travel speed (mm/min)	800
Focus distance (mm)	20
Laser spot diameter on the workpiece (mm)	5
Laser shield gas (L/min) - Argon	8
Powder feed rate (g/min)	30
Nozzle type	coaxial
Nozzle angle (⁰)	90
Laser Power (kW)	1.0 to 4.0
Laser Power Step (kW)	0.5

3. Results and Discussion

3.1 Bead geometry and dilution

Figure 4 presents the macrographic analysis of the Hastelloy C276™ as single bead coatings deposited on both substrates. It is suitable to highlight that the coatings showed no welding defects, following previous work[3]. Moreover, the different burn-in shape was observed in this study. Shallow and uniformly molten substrate areas were induced when 1.5 kW laser power was applied. Besides that, from 2.0 to 4.0 kW under the influence of the Gaussian laser energy distribution and, as a consequence of power

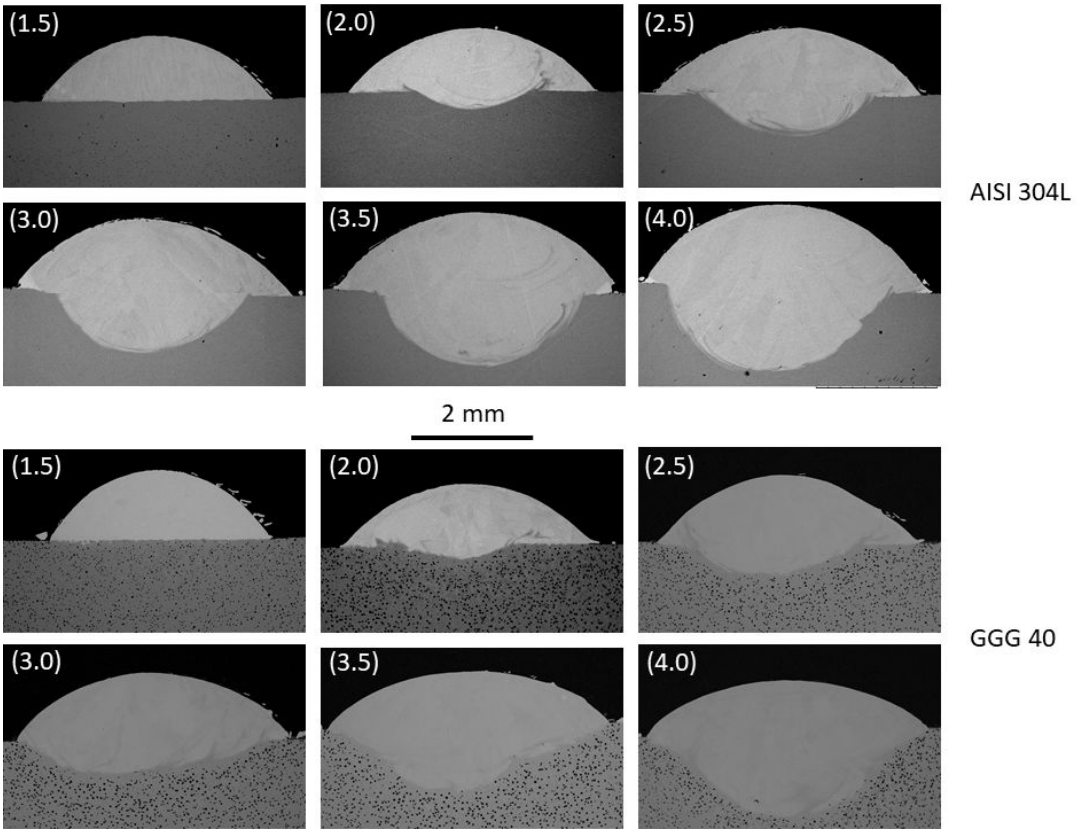

Figure 4. Hastelloy C276™ single beads macrography with the respective laser power (kW) and substrate.

concentration in the middle of the laser spot (or bead), different intensity of burn-in shape was verified, following earlier reports[15]. According to the same authors, the higher the burn-in region, the higher the dilution with the substrate.

Table 3 shows the single bead geometry measurements, based on the cross-section images (see Figure 4). Wettability angle ranged from 46 and 50° for coatings on AISI 304L stainless steel and from 43 to 57° for coatings on GGG 40 ductile iron. On the contrary to the observed for coatings processed by plasma transferred arc (PTA)[3,6,16], in which there was a clear trend between deposition current (or heat input) and the wettability angle –lower contact angle was observed for higher heat inputs – in the case of laser cladding studied in this work, there was no obvious tendency. Otherwise, the bead width increases as laser power increases, approaching the nominal laser spot size on the workpiece (5 mm) when higher laser intensity was applied. This is attributed to the Gaussian laser energy distribution as was reported by other authors[15]. In this way, reinforcement thickness (or clad height) showed only little change and, despite having some oscillations, values closely ranged around 1 mm, pointing out the laser power is a weak parameter in influencing of clad height[17].

The dilution with the substrate was calculated in the cross-section area by the area's method[3], as can be seen in Figure 5. Analogously, dilution was also determined by

Table 3. Wettability angle (θ), bead width (W) and reinforcement thickness (t) measurements for all laser power tested on both substrates.

Substrate	Laser Power (kW)	θ (°)	W (mm)	t (mm)
AISI 304 L	1.5	50	3.9	1.1
	2.0	49	4.1	1.1
	2.5	46	4.4	1.1
	3.0	48	4.7	1.2
	3.5	49	4.7	1.3
	4.0	49	4.8	1.3
GGG 40	1.5	57	3.7	1.2
	2.0	43	4.2	1.0
	2.5	43	4.4	1.1
	3.0	54	4.5	1.1
	3.5	50	4.7	0.9
	4.0	48	4.7	0.9

the iron content adopting Toyserkani method [8], as seen in Figure 6. Both dilution measurement techniques showed good correlation and close values and tendencies for the systems studied. It is important to highlight, especially for the lowest laser power condition, that the dilution values showed the highest percentual difference between the methods. It seems plausible to say that the area´s method reached the accuracy limit, due to the very small substrate molten area.

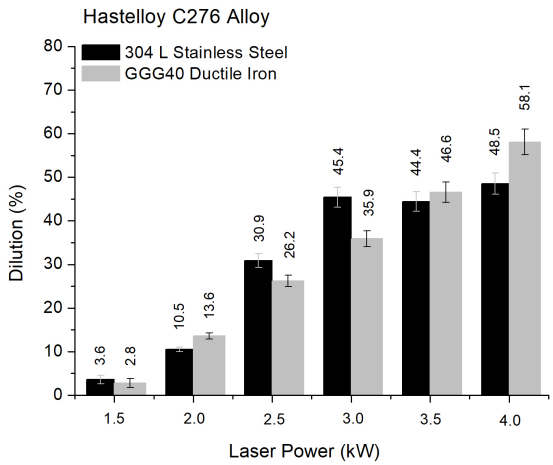

Figure 5. Typical dilution by areas method[3].

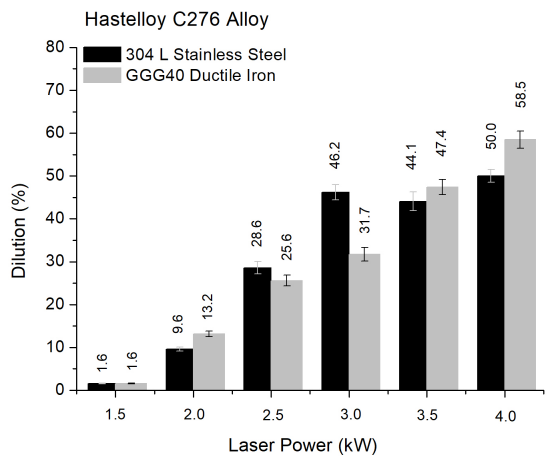

Figure 6. Typical dilution by Toyserkani method[8].

From 3.0 kW on, dilution on AISI 304L stainless steel substrate has shown values reaching a plateau. Differently, such a tendency was not observed for coatings processed on GGG40 ductile iron. It is reasonable to purpose here that the different laser absorptivity of the substrates influenced the dilution results. According to Haldar and Saha[10], processing of high laser reflective materials may cause damage to the machine components due to intense back reflection of the laser beam. In this work, pronounced back reflection was observed when processing coatings on stainless steel at higher powers and the polymeric torch feeding pipes needed to be protected with reflective material, reinforcing the effect of substrate on the laser absorptivity/reflectivity and, hence influencing the dilution on AISI 304 L.

3.2 Coatings microstructure and phase description

XRD spectra (Figure 7) shows the formation of different carbides on Ni - γ (FCC) matrix. Two chromium carbides were identified, namely $M_{23}C_6$ and M_7C_3 where M is chromium. The lower thermal conductivity of the stainless steel and therefore the slower cooling rates during solidification induced the formation of the most thermodynamic stable second phase in the coating, in this case, $M_{23}C_6$ [Cr]. Otherwise, Cr_7C_3 was the phase identified in coatings deposited on ductile iron because of the higher thermal conductivity and thus, faster cooling rates during solidification. Zhong and Liu[9] have reported that the laser cladding process, kind of substrate and its dimensions create solidification conditions out of the thermodynamic equilibrium. Ferreira et al.[3] observed similar phases when processing Hastelloy C276 coatings by plasma transferred arc on AISI 316 L stainless steel, corroborating with the results presented. Thereby, this work confirmed and highlighted the influence of substrate chemical composition on the type of chromium carbide formed due to its direct effect on the heat dissipation.

A further effect of dilution and substrate on the second phase formation was also noticeable when analyzing MC and M_6C carbides, where M is iron, molybdenum or tungsten. Concerning the lowest dilution, M_6C carbides were

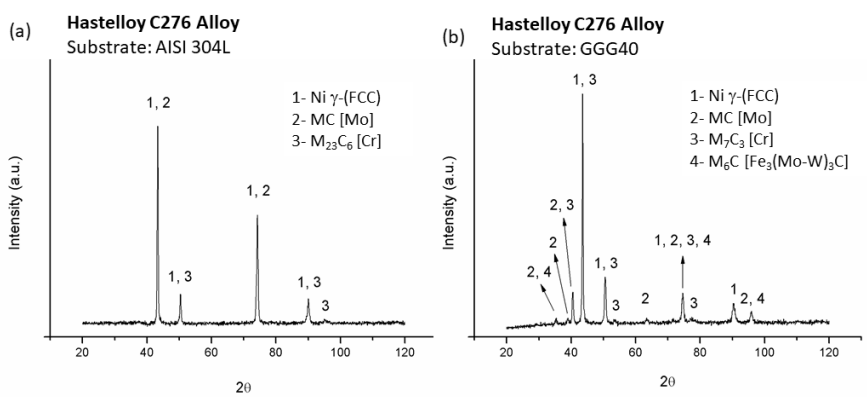

Figure 7. Typical X-ray diffractograms for coatings on: (a) AISI 304L (2.0 to 4.0 kW) and (b) AISI 304L (1.5 kW) and GGG40 (1.5 to 4.0 kW).

formed independently of the chosen substrate. However, as dilution increases, blocky MC carbides were predominantly formed in spite of M_6C (Figure 7a) for the AISI 304L substrate due to its lower carbon content. Finally, it was seen from Figure 7b that M_6C carbide ($Fe_3(Mo\text{-}W)_3C$) is the dominant second phase as a consequence of a large introduction of carbon and silicon from the ductile iron substrate (nominal C: 3.9 wt% and Si: 2.8 wt%). Results followed previous reports about the effect of these elements on carbide morphology in superalloys microstructure[3,5,18].

As can be seen in Figure 8 and Figure 9, the microstructure is comprised of Ni - γ (FCC) dendrites and an interdendritic region containing different carbide fraction. Taking into account the extremely refined microstructures, further

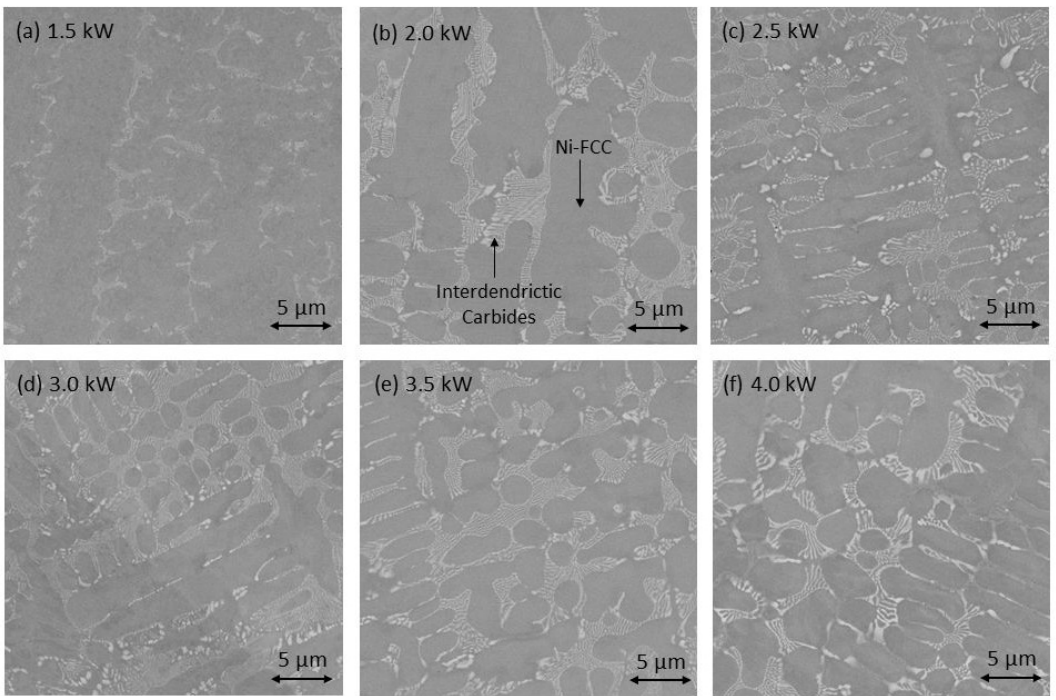

Figure 8. The microstructure of coatings deposited on GGG 40 *versus* laser power.

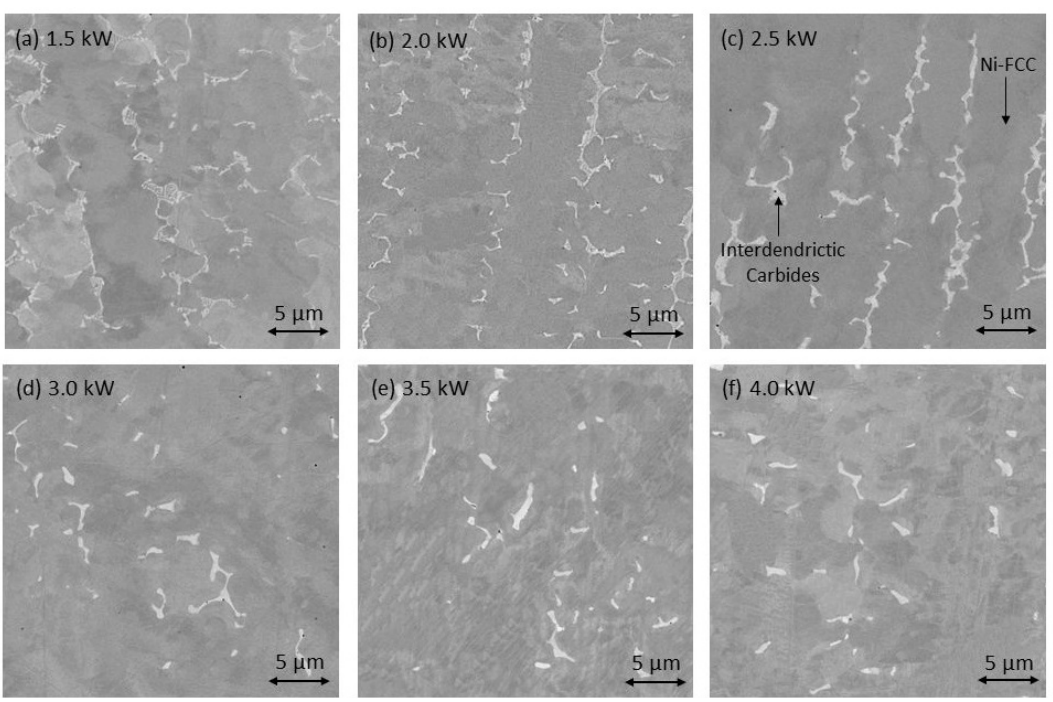

Figure 9. The microstructure of coatings deposited on 304 L *versus* laser power.

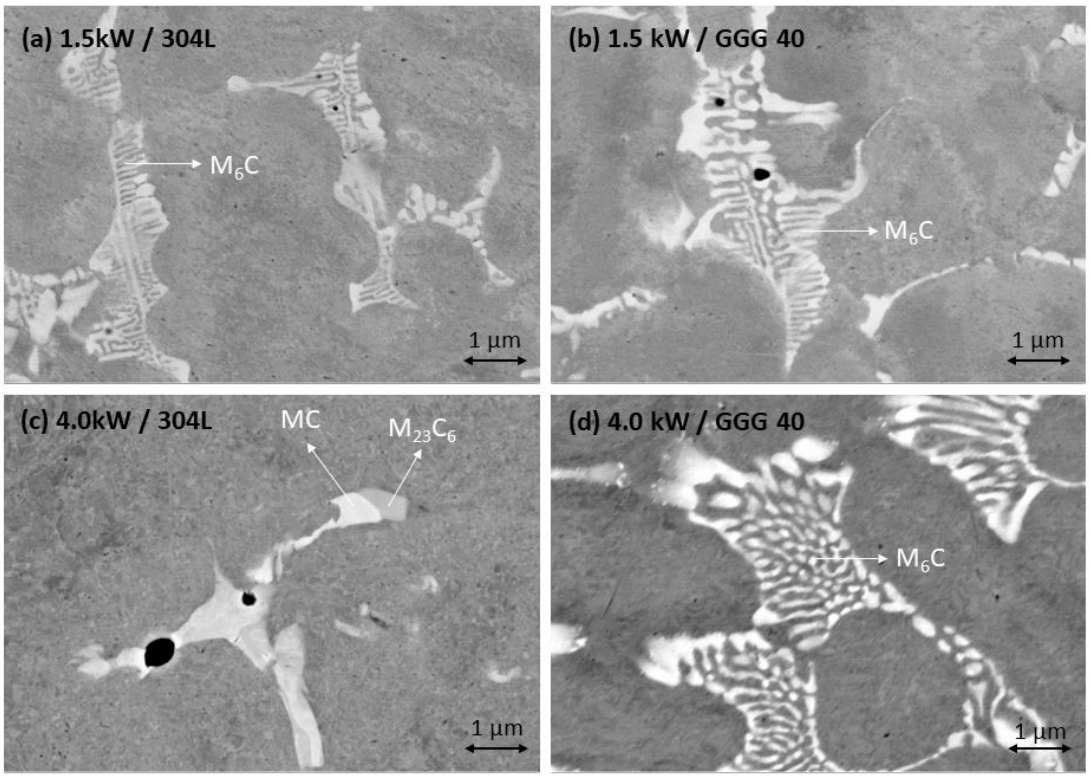

Figure 10. The detailed evaluation of the coating´s carbide.

characterization in a high-resolution field emission gun Scanning Electron Microscope (FEG-SEM) was performed, as seen in Figure 10. For the lowest diluted specimens, lamellar eutectic (Fe3(Mo-W)3C) carbides were formed on both substrates as a dominant second phase (Figure 10ab). As dilution increases in coatings on ductile iron, the carbide fraction increased, but the morphology did not change, remaining as lamellar-like M_6C carbide (Figure 10d). On the other hand, as the dilution increases on stainless steel, the main carbides changed to a mix of $Cr_{23}C_6$ and MoC in a blocky-like morphology (Figure 10c).

Concerning now the coatings microstructure and phase differences observed, the further investigation involved the effect of processing on strengthening mechanisms. Thus, alloying elements were measured by EDS and the phase fraction was evaluated by Image J™[14], as shown in Figure 11 and Figure 12. According to Ferreira, Graf and Scheid[3], the dilution with the stainless steel led to a reduction of important solid solution alloying elements, i.e. molybdenum and tungsten. Similarly, and as AISI 304L has higher chromium content than Hastelloy C276 alloy, higher chromium content was measured.

On the contrary, coatings deposited on GGG40 ductile iron showed an overall reduction in the superalloy alloying elements (Cr, Mo, and W). Thus, the higher the dilution, the lower the solid solution alloying in the coatings, following previous studies[3,6,16].

A reduction of the carbide fraction was observed for coatings on AISI 304L, as a consequence of the low carbon content of the substrate. Besides that, the introduction of carbon and silicon from the GGG40 induced the increase of carbide fraction comparatively with the lowest dilution condition, following what Ferreira, Graf and Scheid[3] observed for Hastelloy C276 deposits on API 5L X70 high strength low-alloy steel. The same authors attributed the carbide fraction increases due to the higher carbon content of the steel substrate. In summary, the results observed in the present work revealed the weakening of both strengthening mechanisms for coatings on stainless steel. A contrary trend on the mechanisms was verified for coatings on ductile iron, i.e. decreasing the solid solution alloying and increasing the second phase fraction.

Additionally, Zhong and Liu[9] reported that the cooling rate in laser cladding can reach 10^3 to 10^7 K/s, depending on the process parameters, substrate type, and dimensions. The same authors mentioned that very fine solidification microstructures were observed as a result of high cooling rates, altering the primary and secondary dendritic arm spacing or - in eutectics - the distance of interlamellar spacing. The investigation about the secondary dendritic arm spacing (DAS) on the coating's microstructure was carried out adopting the methodology purposed earlier by Paes and Scheid[16], despite being the present analysis limited by the larger and variable interdendritic carbide volume fraction. DAS measurements for Hastelloy C276 coatings by laser cladding showed values ranging between 1.4 and 2.7 µm on average. These results are notably lower than those determined for the same alloy coatings processed by plasma transferred arc (i.e. DAS: 6 to 13 µm)[3], confirming the influence of the process on the microstructure refinement.

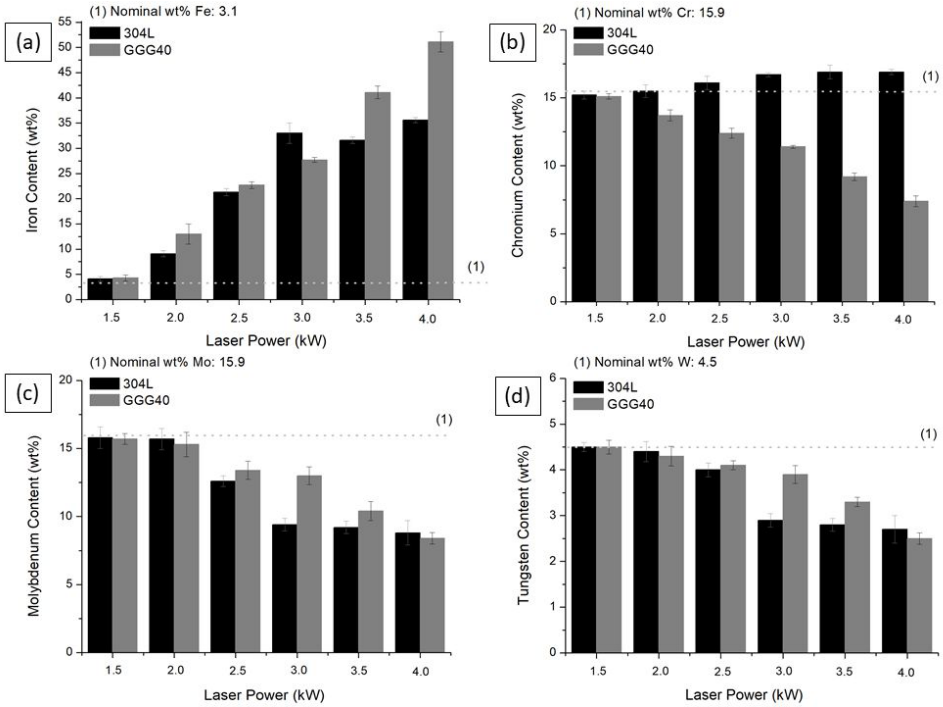

Figure 11. Alloying elements' content measured by EDS *versus* laser power.

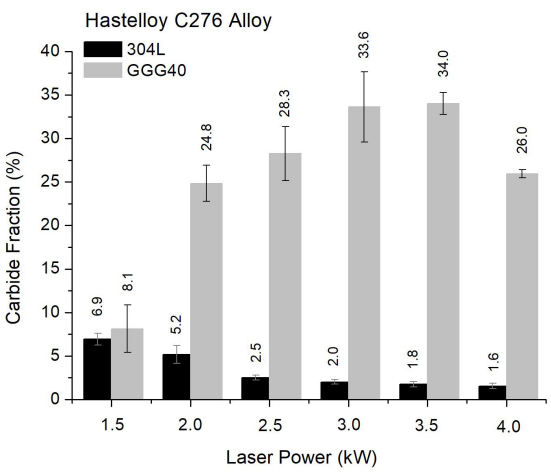

Figure 12. Carbide phase fraction for different conditions.

3.3 Coatings hardness and wear behavior

Considering the shreds of evidence around the effect of processing and kind of substrate on the microstructure and strengthening mechanisms, coatings hardness was evaluated, as seen in Figure 13.

Higher dilution promoted hardness decrease for coatings on AISI 304L, following previous reports about the effect of dilution on the coating's features[3,6,16]. The authors argued about the effect of reduction of both solid solution alloying and carbide fraction when superalloys are deposited on austenitic stainless steel. However, comparing the hardness value (300 HV) obtained in this work for Hastelloy C276 coatings with low dilution with the same alloy coatings processed by PTA on API 5L X70 (dilution < 5%: 270 HV)[3], it is quite easy to explain the difference based on the microstructure refinement. As the laser power increases, the higher dilution promotes a reduction in the coating hardness.

Otherwise, dilution increase pointed out to an interesting and different effect on the coatings processed on GGG 40 ductile iron. In this case, despite showing a reduction in solid solution alloying elements (see Figure 11), carbide fraction was significantly increased up to 3.5 kW (Figure 12) as a consequence of higher carbon and silicon diluted from the substrate. After that, despite introducing an even higher amount of carbon and silicon, the reduction of alloying elements (carbide formers) limited the further fraction increase. Therefore, coatings on GGG 40 showed a hardness increase up to 45% as a consequence of the carbide fraction which in turn reached up to 4 times higher than the lowest diluted condition.

For the lowest dilutions (< 5% or close to zero, see Figure 5 and Figure 6), a similar wear rate was found regardless of the substrate, as can be seen in the 1.5 kW plots in Figure 14. The results can be explained by the microstructure similarities, including carbide fraction and the amount of solid solution alloying elements, as previously discussed. Furthermore, the hardness values are roughly the same for these coatings, which in turn reinforces the expected wear rate behavior. Ferreira, Graf and Scheid[3], studied Hastelloy C276 alloy coatings by PTA deposited on different substrates. The authors showed an increase in the wear rate as the dilution increased. However, in the present study, Hastelloy C276 alloy coatings by laser on ductile iron (GGG 40 / 4.0 kW, Figure 14) showed a different trend and will be further discussed.

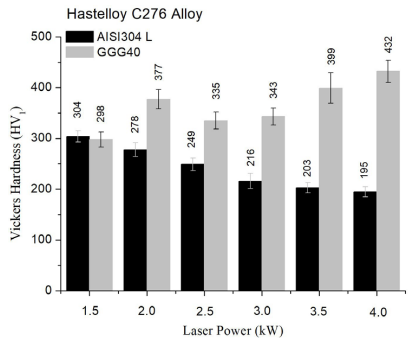

Figure 13. Vickers hardness of the coatings.

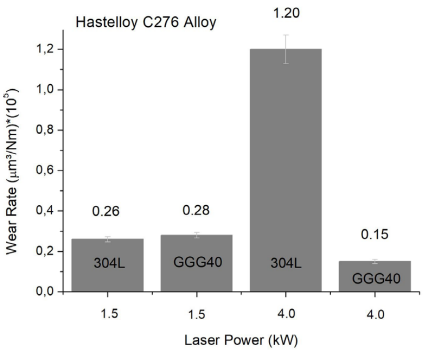

Figure 14. Wear rate of coatings *versus* laser power.

Taking into account the highest dilution specimens the effect of the substrate on the coating's features are noticeable. Deposits on AISI 304L by 50% dilution showed the highest wear rate, reaching 5 times the wear rate of samples with dilution lower than 5%. Such behavior can be supported by the reduction in the carbide fraction (see Figure 12), as well as in the amount of molybdenum and tungsten (see Figure 11) which restrain the solid solution hardening effect.

Finally, the analysis of the coatings on ductile iron (58% dilution) showed that, despite the significant reduction of solid solution hardening elements (Mo and W), the introduction of carbon and silicon from the substrate led to a high carbide fraction, which became the dominant strengthening mechanism. Thus, the wear rate was reduced by 45% when compared to the alloy coatings with low dilution, where the hardening effect is less pronounced.

Additional evaluation on the wear tracks for low dilution on both substrates (1.5 kW) and high dilution on 304L (4.0 kW) showed the presence of darkened regions, as shown in Figure 15. It is noteworthy that oxygen, molybdenum, and chromium were identified by EDS spectroscopy on the dark areas, suggesting oxidation of the surface during the ball-on-flat sliding wear tests, as seen in detail in Figure 15cd. It is important to highlight that the formation of these oxides more intensely occurred on the low dilution conditions and also under high dilution on AISI 304L since the chromium content is high too. Hence, it can be concluded that, in

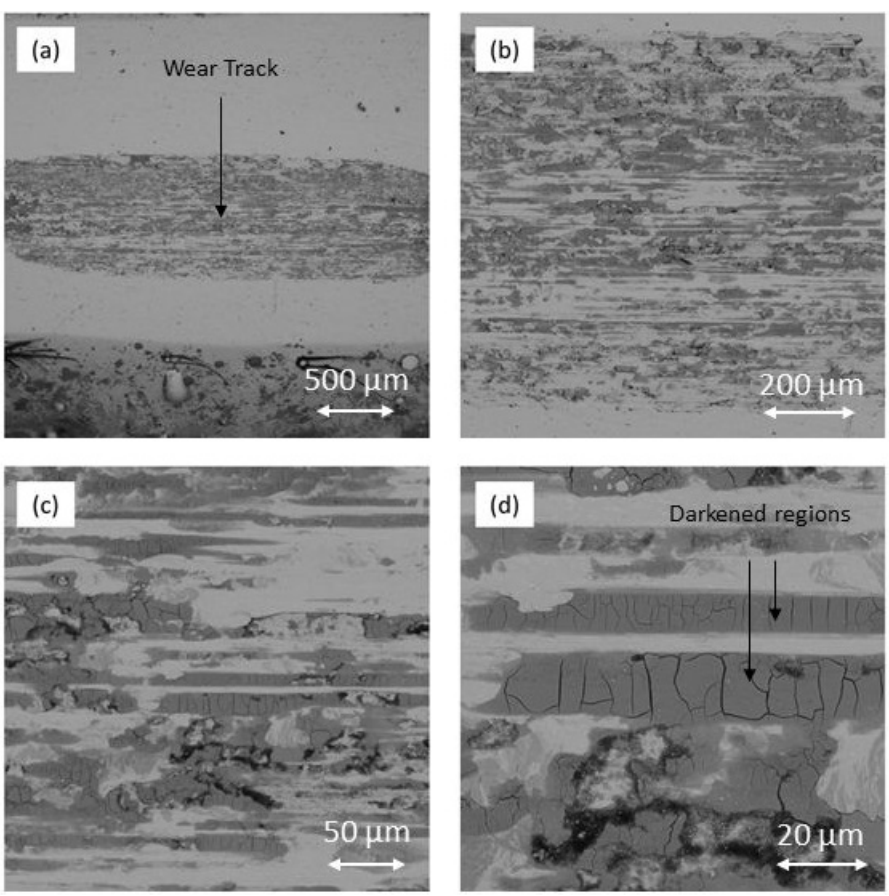

Figure 15. Typical wear tracks of coatings deposited with 1.5 and 4.0 kW on AISI 304L and 1.5kW on GGG40.

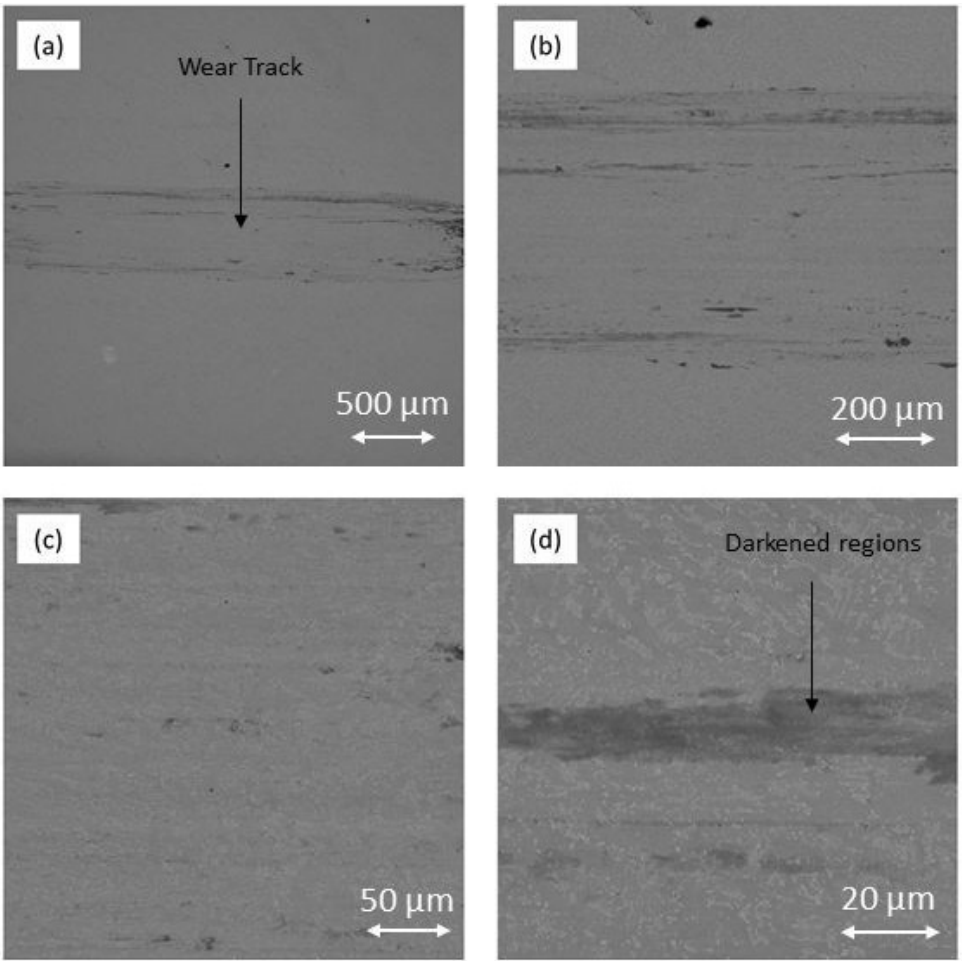

Figure 16. Typical wear tracks of coatings deposited with 4.0 kW on GGG40.

addition to the fact that the mentioned conditions show the lower hardness, surface oxidation during the wear test led to the development of an even more aggressive scenario, resulting in higher wear rates.

Mishra et al.[19] reported the oxidation influence on the wear behavior of Ni-base superalloys. Oxidation may be providing a protective layer inhibiting the metal-metal contact and, otherwise, sometimes oxide particles could act as abrasives accelerating the wear of the rubbing surfaces. The report[19] reinforces the suggested mechanism identified in the present research (previous sentence) and, besides, it was observed here that the surface showed a wear process with a successive growth and delamination of the oxide layer generated into the wear track because of interaction between asperities, following what suggested Navas et al.[20] in their studies about cobalt-base superalloy. Haseeb, Albers and Bade[21] also studied friction and wear behavior of nickel-tungsten alloy films and reported that a considerable amount of oxygen on nickel wear tracks indicate oxidation during the wear test.

Finally, the analysis of the wear tracks for the highest heat input coatings on GGG40 - the best wear performance condition - pronouncedly indicated a reduction in the oxidation process, as shown in Figure 16. In addition to the high hardness of the coating, there was virtually no surface oxidation, resulting in the lowest wear rate. Such behavior can be explained by the high dilution, which induces a significant reduction in the content of the oxide-forming elements, besides inducing the formation of a high fraction of wear-resistant carbides.

4. Final Remarks

The effect of laser power and kind of substrate on the microstructure and properties of Hastelloy C276 alloy coatings by laser cladding were assessed. The main conclusions can be presented:

- Despite adopting hugely different substrates, the set-up of the laser cladding process when aiming low dilution can deliver highly similar coatings with comparable microstructure, phase-type, and distribution, hardness and wear behavior.
- Considering a certain degree of dilution, the type of substrate significantly rules the second phase nature and fraction in the Hastelloy C276 alloy coatings. Hence, coatings on AISI 304L prevailed formation of $M_{23}C_6$ (Cr) and MC (Mo) blocky-like carbides and, while, deposits on GGG40 induced to M_7C_3 (Cr) and MC (Mo) with a prevalent M_6C lamellar-like carbide. It highlights the effect of

substrate composition and thermal conductivity on coatings microstructure.

- Coatings deposited on GGG40 ductile iron showed significant hardening as the laser power increased (higher dilution). It was due to carbide fraction increase, a mechanism that overwhelmed the reduction of important solid solution hardening elements. The microstructure modifications notably enhanced the wear performance of these coatings.
- The effect of the dilution has clearly shown the importance of predicting and interpreting the coating´s microstructure. Dealing with the deposition system - in this case, the laser power and kind of substrate - this work emphasized how attractive is to research the possibilities of coating design.

5. Acknowledgments

The authors thank SENAI Institute for Innovation (ISI Joinville) for the support of laser processing and characterization.

6. References

1. Venkatesh B, Sriker K, Prabhakar VSV. Wear characteristics of hardfacing alloys: state-of-art. Procedia Materials Science. 2015;10:527-32. http://dx.doi.org/10.1016/j.mspro.2015.06.002.
2. Mankins WL, Lamb S. Nickel and nickel alloys. In: ASM International. Properties and selection: nonferrous alloys and special-purposed materials. Ohio: Materials Park; 1990. p. 1363-403.
3. Ferreira LS, Graf K, Scheid A. Microstructure and properties of nickel-based C276 alloy coatings by PTA on AISI 316L and API 5L X70 steel substrates. Mater Res. 2015;18(1):212-21. http://dx.doi.org/10.1590/1516-1439.332914.
4. Fernandes F, Cavaleiro A, Loureiro A. Oxidation behavior of Ni-based coatings deposited by PTA on gray cast iron. Surf Coat Tech. 2012;207:196-203. http://dx.doi.org/10.1016/j.surfcoat.2012.06.070.
5. Graf K, Tetzlaff U, Souza GB, Scheid A. Effect of dilution on the microstructure and properties of cocrmosi alloy coatings processed on high-carbon substrate. Mater Res. 2019;22(1):e20180502.
6. Antoszczyszyn TJ, Paes RMG, Oliveira ASCM, Scheid A. Impact of dilution on the microstructure and properties of Ni-based 625 alloy coatings. Soldag Insp. 2014;19(2):134-44. http://dx.doi.org/10.1590/0104-9224/SI1902.05.
7. Paes RMG, Martinazzi D, Falcade T, Scheid A. Effect of bead overlapping on the microstructure and mechanical properties of CoCrWC alloy coatings. Mater Res. 2018;21(6):e20180274. http://dx.doi.org/10.1590/1980-5373-mr-2018-0274.
8. Toyserkani E, Khajepour A, Corbin S. Laser cladding. Washington: CRC Press; 2005. p. 179-224.
9. Zhong M, Liu W. Laser surface cladding: the state of the art and challenges. Proc Inst Mech Eng, C J Mech Eng Sci. 2010;224(5):1-20. http://dx.doi.org/10.1243/09544062JMES1782.
10. Haldar B, Saha P. Identifying defects and problems in laser cladding and suggestions of some remedies for the same. Materials Today: Proceedings. 2018;5(2):13090-101. http://dx.doi.org/10.1016/j.matpr.2018.02.297.
11. Mahamood RM. Laser metal deposition process of metals, alloy, and composite materials. Cham: Springer International Publishing; 2018. http://dx.doi.org/10.1007/978-3-319-64985-6.
12. DIN: Deutsches Institut für Normung. DIN 1693-1:1973: cast Iron with nodular graphite: unalloyed and low alloy grades. Berlin: DIN; 1973.
13. Abioye TE, McCartney DG, Clare AT. Laser cladding of Inconel 625 wire for corrosion protection. J Mater Process Technol. 2015;217:232-40. http://dx.doi.org/10.1016/j.jmatprotec.2014.10.024.
14. Rasband WS. Image J [Internet]. Bethesda: U. S. National Institutes of Health; 2015 [cited 2018 Mar 20]. Available from: http://imagej.nih.gov/ij/
15. Goodarzi DM, Pekkarinen J, Salminen A. Effect of process parameters in laser cladding on substrate melted areas and the substrate melted shape. J Laser Appl. 2015;27(S29201):1-9. http://dx.doi.org/10.2351/1.4906376.
16. Paes RMG, Scheid A. Effect of deposition current on microstructure and properties of CoCrWC alloy PTA coatings. Soldag Insp. 2014;19(3):247-54. http://dx.doi.org/10.1590/0104-9224/SI1903.07.
17. Lawrence J, Pou J, Low DKY, Toyserkani E. Advances in laser materials processing, technology, research, and application. Washington: Woodhead; 2010. p. 426-57. http://dx.doi.org/10.1533/9781845699819.
18. Jiang L, Zhang WZ, Xu ZF, Huang HF, Ye XX, Leng B, et al. M_2C and M_6C carbide precipitation in Ni-Mo-Cr based superalloys containing silicon. Mater Des. 2016;112:300-8. http://dx.doi.org/10.1016/j.matdes.2016.09.075.
19. Mishra SB, Chandra K, Prakash S. Dry sliding wear behavior of nickel-, iron- and cobalt-based superalloys. Tribology. 2013;7(3):122-8. http://dx.doi.org/10.1179/1751584X13Y.0000000038.
20. Navas C, Cadenas M, Cuetos JM, Damborenea J. Microstructure and sliding wear behavior of Tribaloy T-800 coatings deposited by laser cladding. Wear. 2006;260(7-8):838-46. http://dx.doi.org/10.1016/j.wear.2005.04.020.
21. Haseeb ASMA, Albers U, Bade K. Friction and wear characteristics of electrodeposited nanocrystalline nickel–tungsten alloy films. Wear. 2008;264(1-2):106-12. http://dx.doi.org/10.1016/j.wear.2007.02.004.